Accepted for publication Journal of Dynamic Systems, Measurements, and Control, ASME Publications.

Modelling and Parameter Identification of Harmonic Drive Systems

H.D. Taghirad and **P.R. Bélanger**

Center for Intelligent Machines,

Department of Electrical Engineering,
McGill University, Montréal, H3A 2A7

Abstract

The unique performance features of harmonic drives, such as high gear ratios and high torque capacities in a compact geometry, justify their widespread industrial application, especially in robotics. However, harmonic drives can exhibit surprisingly more complex dynamic behavior than conventional gear transmissions. In this paper, a systematic way to capture and rationalize the dynamic behavior of the harmonic drive systems is examined. Simple and accurate models for compliance, hysteresis, and friction are proposed, and the model parameters are estimated using least–squares approximation for linear and nonlinear regression models. A statistical measure of variation is defined, by which the reliability of the estimated parameter for different operating condition, as well as the accuracy and integrity of the proposed model is quantified. Finally, the model performance is assessed by a simulation verifying the experimental results on two different harmonic drives.

1 Introduction

Since its inception in 1955, the harmonic drive has found widespread acceptance among practitioners. This mechanical transmission, occasionally called "strain-wave gearing", employs a continuous deflection wave along a *non-rigid gear* to allow for gradual engagement of gear teeth. Because of this unconventional gear-tooth meshing action, harmonic

drives can deliver high reduction ratios in a very small package. In fact, the radical mechanical operation of this gear train defies conventional understanding of gear behaviour and creates a new arena for exploration and understanding.

The harmonic drive exhibits performance features both superior and inferior to those of conventional gear transmissions. Its performance advantages include high torque capacity, concentric geometry, lightweight and compact design, near–zero backlash, high efficiency, and back drivability. Harmonic drive systems suffer however, from high flexibility, resonance vibration, friction and structural damping nonlinearities. The unique performance features of the harmonic drive have captured the attention of designers in many fields. It has been used in industrial and space robots, assembly equipment, and measuring instruments, as well as heavy duty applications such as machine tools and printing presses. Additionally, space and aircraft systems often employ harmonic drives for their light weight and compact geometry.

Throughout its short existence, the harmonic drive has enjoyed increasing international attention from designers as well as researchers. The Russians were perhaps the first who initiated substantial research on the dynamic behavior of harmonic drives [1, 24].

More recently Tuttle and Seering performed an extensive effort to model the stiffness, positioning accuracy, gear tooth-meshing mechanism and friction of the harmonic drive [22, 23]. Their experimental observations show that the velocity response to step commands in motor current are not only contaminated by serious vibration, but also by unpredictable jumps. The velocity response observations were used to guide the development of a series of models with increasing complexity to describe the harmonic drive behavior. Their most complex model involved kinematic error, nonlinear stiffness, and gear-tooth interface with frictional losses.

Kircanski and Goldenberg have also attempted to model the harmonic drive in detail [13]. They used the drive system in contact with a stiff environment, in contrast to unrestrained motion experiments used by Tuttle and Seering [23], and illustrated that in this case nonlinear stiffness, hysteresis and friction are more tractable. Simple models for soft-windup, hysteresis, and friction were proposed and the parameters were identified by restrained motion experiments.

Hsia [11], Legnani [14], Marilier [16], and Seyfferth [17] are among others who attempted to model the stiffness, friction, and position accuracy of harmonic drive systems. All these researchers noted the inherent difficulties in finding an accurate model for the system.

In this paper a moderately complete model of harmonic drive system is developed. Restrained and unrestrained motion experiments are use to identify the model parameters and illustrate the fidelity of the model for two different types of harmonic drive systems. It is shown that a linear stiffness model for stiffness combined with a velocity dependent structural damping model can replicate the hysteresis torsion curve of the system compliance. The frictional losses of the transmission have been modelled using Coulomb friction, viscous damping and Stribeck friction. Both high speed, and low speed friction terms have been identified using unrestrained and restrained motion experiments respectively. Finally, the simulation of the system, built in Simulink, has been used to verify the model fidelity by experiments. It has been verified that the simulation accurately predicts the restrained and unrestrained experiments.

2 Experimental Setup

Two harmonic drive testing stations were used to monitor the behaviour of two different harmonic drives. A picture of those setups is illustrated in Figure 2, in which the harmonic drive is driven by a DC motor, and a load inertia is used to simulate the robot arm for unrestrained motion. Also a positive locking system is designed such that the output load can be locked to the ground for restrained motion experiments. In the first setup, a brushed DC motor from Electro–Craft, model 586-501-113, is used. Its weight is 1.36 Kg, with maximum rated torque of 0.15 Nm, and torque constant of 0.0543 Nm/amp. The servo amplifier is a 40 Watts Electro–Craft power amp model Max-100-115. The harmonic drive in this setup is from RHS series of HD systems model RHS-20-100-CC-SP, with gear ratio of 100:1, and rated torque of 40 Nm. In the second setup the DC motor is a brushless Kollmorgen Inland motor, model RBE-01503-A00. Its weight is 475 gr, with maximum rated torque of 5.6 Nm, and torque constant of 0.1815 Nm/amp. The servo amplifier is a FAST Drive Kollmorgen, model FD 100/ 5E1. The harmonic drive is from CFS series of HD Systems, Inc. with gear ratio 160:1, and rated peak torque of 178 Nm.

In the first experimental setup, the circular spline is fixed to the ground and the output is carried by the flexspline, while in the other setup, the flexspline is fixed and the circular spline is used for output rotation. By this arrangement, the behavior of the transmission under different operating configurations can be examined. Each setup is equipped with a tachometer to measure the motor velocity, and an encoder on the load side to measure the output position. The output torque is measured by a Wheatstone bridge of strain

gauges mounted directly on the flexspline [19], and the current applied to the DC motor is measured from the servo amplifier output. These signals were processed by several data acquisition boards and monitored by a C-30 Challenger processor executing compiled computer C codes.

3 Modelling and Identification

The goal of modelling the harmonic drive system is to discover the simplest representation which can replicate system performance to a desired level of accuracy. Our purpose in modelling is to implement a model–based torque control algorithm on the system. Moreover, we used the computer model for examining and improving control laws, before implementing them. As recommended by other researchers [13, 23], in order to comply this objective it is necessary to have at least a simple and accurate model for friction, and compliance of harmonic drive systems. In practice it has been proven that the knowledge obtained through the process of modelling and identification of the system becomes a powerful medium for understanding, and improving the design, as well as for providing new horizons for controller design.

3.1 DC Motor

A DC motor can be viewed as a two–input, one–output black box, where the servo current and external torque are the inputs and the angular displacement (or velocity) is the output. The torque balance for the DC motor can be written in the form:

$$K_m i = J_m \ddot{\theta} + T_{f_m} + T_{out} \tag{1}$$

where K_m is the motor torque constant, i is the input current to the motor, J_m is the motor inertia, and T_{out} is the external torque. T_{f_m} is the friction torque, which can be modelled in the form of velocity direction dependent viscous and Coulomb friction as follows:

$$T_{f_m}(\dot{\theta}) = T_{v_n} u_{-1}(-\dot{\theta})\dot{\theta} + T_{v_p} u_{-1}(\dot{\theta})\dot{\theta} + T_{s_n} u_{-1}(-\dot{\theta})\text{sign}(\dot{\theta}) + T_{s_p} u_{-1}(\dot{\theta})\text{sign}(\dot{\theta}) \tag{2}$$

where

$$u_{-1}(x) = \begin{cases} 1 & \text{if } x > 0 \\ 0 & \text{if } x \leq 0 \end{cases} \tag{3}$$

Note that the indices p and n represents the dependence of the friction coefficients on the velocity direction.

	DC Motor 1		DC Motor 2	
	Estimated Parameter	Variation Measure	Estimated Parameter	Variation Measure
K_m	0.0542	0%	0.1815	0%
J_m	5.5×10^{-5}	0.82%	5.8×10^{-5}	5.75%
T_{v_p}	5.3×10^{-5}	23.3%	8.6×10^{-4}	7.75%
T_{v_n}	5.3×10^{-5}	11.5%	5.8×10^{-4}	14.4%
T_{s_p}	1.4×10^{-2}	9.01%	1.5×10^{-2}	25.9%
T_{s_n}	1.3×10^{-2}	5.72%	2.7×10^{-2}	25.8%

Table 1: DC motors estimated parameters

The model parameters are estimated by least–squares approximation. Using Equation 1 as a linear regression model, and measuring the motor velocity and current for two sets of high and low velocity experiments, the model parameters can be estimated using the *Moore–Penrose generalized inverse* [7, 4]. Householder reflection is utilized in numerical calculations to avoid ill conditioning [8].

Four type of inputs are applied to the servo amplifier, and motor velocity and current are measured and logged in each experiment. The input shape functions are sinusoid, square wave, triangular wave, and composite sine wave, where the composite sine waves are generated combining three sinusoids as: $\cos(\omega t) + 0.5\ \sin(2\omega t) + \sin(3\omega t)$. For each signal type, frequencies from 0 to 10 Hz and amplitude from 10 % to 100 % of maximum allowable amplitude are spanned, to experiment both low and high velocities with wide frequency range. To generate the motor acceleration from the velocity signal, first the velocity signal are filtered using a fifth order Butterworth filter, by zero-phase distortion routine, and then numerically differentiated. The details and advantages of this method are analysed through simulation and reported in [18].

By means of least–squares estimation, for each experiment we obtained a set of parameters. However, these parameters are deemed acceptable, only if they are consistent between experiments. This can be quantified by a statistical measure, namely *the ratio of the standard deviation to the average value of each parameter estimated for different experiments* which we call *variation measure*. If the variation measure is small, we have good consistency for different experiments, and model is capable of capturing the dynamics of the system.

Figure 3 illustrates the velocity fit obtained by the model for two typical experiments. The model is able to capture the dynamics of the system for both low and high velocity

experiments. Table 1 summarizes the estimation results for two setup DC motors, where for each setup about 15 experiments are considered (All parameters expressed in SI units). The motor torque constant K_m is obtained from the motor specs, and assumed to be known in the least–squares estimation. The variation measure of the results for different experiment shows less than 10% for some parameters, and less than 30% in others. The reason for variation in variation measure among parameters is that the responses are relatively insensitive to variations in those particular parameters. However, it has been verified by simulations that having variation measure less than 30% gives relatively good match to the experiments [18].

3.2 Harmonic Drive Compliance

As described in a manufacturer's catalogue [12], a typical shape of the harmonic drive compliance curve is given in Figure 4. This curve illustrates harmonic drive nonlinear stiffness and hysteresis. To capture the nonlinear stiffness behavior, manufacturers suggest using piecewise–linear approximations [12], whereas other researchers prefer a cubic polynomial approximation [23, 24]. The hysteresis effect, however, is more difficult to model, and consequently it is often ignored. Recently Seyfferth et al. proposed a fairly complex model to capture the hysteresis [17]. The hysteresis in the harmonic drive compliance profile is caused by structural damping of the flexspline. The inherent coupling of stiffness torque and structural damping, therefore, make it very hard to identify those separately. We suggest that Figure 4 is in fact a Lissajous figure, and we identify both the stiffness and damping of the flexspline together using least–squares estimation. Linear and cubic models for compliance and many different models for structural damping were tried in this framework. The Dahl model for friction [6, 20], the Duham, Preisach and Babuska models for hysteresis [15], are among the dynamic models used to replicate the hysteresis torsion curve. We observed, however, that a linear stiffness model with a static model, relating the structural damping to a power of the velocity can best capture hysteresis behavior. The reason why dynamic models were not capable of predicting hysteresis in harmonic drive structural damping accurately is that despite their dynamic relation, the dependence of the structural damping torque to a power of the velocity was not introduced by them. Hence, our proposed model, simpler in structure, appears to better characterize the hysteresis, and in practice the variation measure of identified parameters in our model is much less than those of other dynamic models we examined. Equation 4 gives in detail

	Harmonic Drive 1		Harmonic Drive 2	
	Estimated Parameter	Variation Measure	Estimated Parameter	Variation Measure
α	$\frac{1}{2}$	0%	$\frac{1}{2}$	0%
K_1	6340	9.6%	104.2	4.36%
T_{st}	57.2	28.2%	7.96	28.0%
J_{eff}	1.0×10^{-4}	6.38%	1.0×10^{-4}	8.72%
T_{v_p}	3.7×10^{-4}	16.7%	1.8×10^{-3}	13.2%
T_{v_n}	3.5×10^{-4}	19.3%	2.1×10^{-3}	8.42%
T_{s_p}	4.6×10^{-2}	23.7%	7.5×10^{-2}	29.2%
T_{s_n}	4.4×10^{-2}	24.0%	3.3×10^{-2}	30.8%
$T_{ss_{p1}}$	-0.0076	14.7%	-0.0487	20.3%
$T_{ss_{n1}}$	-0.0203	23.8%	-0.0450	18.6%
T_{ss_2}	0.1	0%	0.1	0%

Table 2: Harmonic drives estimated parameters

the compliance model, where $\Delta\theta$ is the flexspline relative torsion.

$$T_{meas} = K_1 \Delta\theta + T_{st} |\Delta\dot{\theta}|^{\alpha} \text{sign}(\Delta\dot{\theta}) \tag{4}$$

To identify the model parameters, a set of restrained motion experiments has been employed, in which the torque T_{meas} and the motor velocity have been measured. The experiment shape functions are the same as that explained in DC motor experiments. Equation 4 forms a nonlinear regression in which K_1, T_{st} and α are unknown. Using an iterative least–squares solution for this nonlinear regression model, it is found that the optimal estimate of α is very close to 0.5. Consequently the structural damping can be related to the square root of the relative torsion velocity. Figure 4 illustrates a typical hysteresis torsion curve fitted by the model, comparing the difference between the optimal α and $\alpha = \frac{1}{2}$. The maximum mismatch (points $(-2, -0.5)$ and $(0.5, 0.8)$ in Figure 4) occurs when the velocity is changing rapidly; otherwise, the model is approximating the hysteresis curve quite accurately. By fixing the value of $\alpha = \frac{1}{2}$, Equation 4 forms a linear regression model for the system, that can be solved for different experiments. Table 2 summarizes the compliance parameter for the harmonic drives of our two setups.

3.3 Harmonic Drive Friction

All harmonic drives exhibit power loss during operation due to transmission friction.

Figure 5 illustrates the schematics of the harmonic drive model. The bulk of energy dissipation can be blamed on the wave generator bearing friction T_{f_1}, gear meshing friction T_{f_2}, output bearing friction T_{f_3} and the flexspline structural damping T_{st}. Among them, most of the frictional dissipation results from gear meshing. Also comparing the ball–bearing frictions, T_{f1} is more important than T_{f_3} since it is acting on the high speed/low torque port of transmission, and its effect on the dynamics of the system is magnified by the gear ratio. The transmission torque is measured directly by strain gauges mounted on the flexspline (namely node c_{fs} of Figure 5). The torque balance, therefore, can be written as:

$$T_{wg} = \frac{1}{N}(T_{meas}) + T_{f_1} + T_{f_2} \tag{5}$$

in which the measured torque $T_{meas} = T_k + T_{st}$, N is the gear ratio, and T_{wg} is the resulting torque of wave generator, provided by the DC motor. From Equation 1, T_{wg} can be related to the input current by:

$$T_{wg} = K_m i - J_m \ddot{\theta} - T_{f_m} \tag{6}$$

Thus, the final torque balance of the system is the following:

$$K_m i - \frac{1}{N} T_{meas} = J_{eff} \ddot{\theta}_{wg} + (T_{f_m} + T_{f_1} + T_{f_2}) \tag{7}$$

in which K_m is the motor torque constant, J_{eff} is the effective input inertia, and T_{f_m} is the motor friction. The gear meshing friction torque is modelled as Coulomb, viscous and Stribeck friction [3, 21], having velocity direction dependent coefficient as follows:

$$\begin{aligned} T_{f_2} = {} & T_{v_p} \dot{\theta}_{wg}\ u_{_{-1}}(\dot{\theta}_{wg}) + T_{v_n} \dot{\theta}_{wg}\ u_{_{-1}}(-\dot{\theta}_{wg}) + T_{s_p} \mathrm{sign}(\dot{\theta}_{wg})\ u_{_{-1}}(\dot{\theta}_{wg}) + T_{s_n} \mathrm{sign}(\dot{\theta}_{wg})\ u_{_{-1}}(-\dot{\theta}_{wg}) \\ & + T_{ss_{p1}} \mathrm{sign}(\dot{\theta}_{wg})\ u_{_{-1}}(\dot{\theta}_{wg}) e^{-\left(\frac{\dot{\theta}_{wg}}{T_{ss_{p2}}}\right)^2} + T_{ss_{n1}} \mathrm{sign}(\dot{\theta}_{wg})\ u_{_{-1}}(-\dot{\theta}_{wg}) e^{-\left(\frac{\dot{\theta}_{wg}}{T_{ss_{n2}}}\right)^2} \end{aligned} \tag{8}$$

The Stribeck model for friction can capture the dynamics of the friction at low velocities. Unlike compliance identification, both restrained and unrestrained experiments are employed to identify the friction model parameters. Unrestrained experiments are persistently exciting for viscous and Coulomb friction, while restrained motion experiments operate the system at low velocities which are ideal for Stribeck coefficient identification. Unrestrained low–velocity experiments are used as well, for Stribeck coefficient identification. The experiment shape functions are the same as that explained in DC motor experiments, where for restrained motion case 20 experiments, and for unrestrained motion case 30 experiments are considered for each setup.

Equation 7 forms a linear regression model for the high velocity experiments in the absence of the nonlinear Stribeck terms. It should be noted that in this regression model

instead of the internal system friction T_{f_m}, T_{f_1} and T_{f_2}, the entire friction of the system ($T_f = T_{f_m} + T_{f_1} + T_{f_2}$), can be identified. This imposes no limitation on the identification procedure, since only the entire friction T_f is required for the simulations. For low–velocity experiment also, Equation 7 can provide a linear regression if $T_{ss_2} = T_{ss_{p2}} = T_{ss_{n2}}$ is assumed to be known. Figure 6 illustrates the output torque fit obtained by the model for four typical experiments, assuming fixed $T_{ss_2} = 0.1$. Table 2 summarizes the estimated friction parameters of two harmonic drives, and their variation measure. The variation measure for all parameters are less than 30%, which indicates the reliability of the estimated parameters.

It is important to note that the estimated Stribeck friction coefficients are negative, which is in contrary to the usual dynamics of friction reported at low velocities [2, 10]. Nevertheless, this represents rising friction at low velocities as illustrated in Figure 7, and no stiction, verifying the manufacturers claim [5]. This may be rationalized by the fact that the main bulk of frictional losses in the harmonic drive systems are due to the gear meshing, but that, contrary to other transmissions, a combination of elastic deformation of the flexspline and gear teeth engagement contributes to the velocity reduction. Therefore, the low–velocity experiments in the harmonic drive transmission shows smoother start up velocity compared to the other transmissions. This is verified by both constrained and unconstrained motion experiments, where no stick slip or stiction is observed. The reliability of the negative Stribeck coefficient is assessed first by obtaining acceptable variation measure for Stribeck coefficients, and second by getting similar results for the two different harmonic drives. The effect of noise and other uncertainties at low velocity experiments is also reduced to a minimum by carefully filtering the signals with a fifth order Butterworth filter, by zero–phase distortion routine.

4 Modelling Scheme Verification

To verify model validity, simulations of the system for both restrained and unrestrained systems is developed in Simulink. Figure 8 illustrates the simulation block diagram of the unrestrained motion built in Simulink. The nonlinear equation of motions for each part are embedded in the simulation blocks. A Runge–Kutta fixed–step integration method with $1ms$ integration steps is used to execute the simulation, consistent with the 1 kHz sampling frequency in the experiments. The simulation input is the measured current on the system, as well as the identified parameters reported in Section 3.

One important characteristic of a harmonic drive torque transmission, as observed in unrestrained motion, is a high–frequency oscillation in output torque signal, named torque ripples (See torque curve in Figure 9). Torque ripples are caused mainly by harmonic drive gear meshing vibration. Harmonic drive gear meshing vibrations introduce a real torque oscillation which can be observed in the end effector motions of robots using harmonic drives and even sensed by hand when back–driving the harmonic drive. Its principal frequency of oscillation (in rad/sec) is twice the motor velocity (in rad/sec), since the gear teeth in harmonic drives are meshing in two zones. A small fraction of the torque ripples are caused by the non–ideal torque measurement, because of the direct attachment of strain gauges on the flexspline. Since the flexspline has an elliptical shape, strain gauges mounted on the flexspline are subjected to unwanted strain caused by the elliptical shape. Hashimoto [9], proposed using at least two pairs of Rosette strain gauges to compensate for this unwanted strain. However, ideal compensation is possible only if there is no angular misplacement of strain gauges on the circumference of the flexspline, which is unattainable in practice. It has been found however, that using four Rosset strain–gauges, and using an accurate method to mount the strain–gauges will reduce the amplitude of the torque ripple to a minimum [19]. Unfortunately the frequency of torque ripples (in rad/sec) introduced by the non–ideal behavior of the sensor is also twice the motor speed (in rad/sec), since the major axis of the ellipse is travelling twice as fast as the wave generator. This make it impossible to discern the true ripples caused by the gear meshing vibration from that caused by non–ideal measurement. Power spectral analysis of the observed torque sensor output has confirmed the frequency content of the ripples to be twice the motor speed (in rad/sec), and it shows first–harmonic frequency of four times the motor speed as well. It should be mentioned that to have an accurate model to predict the torque ripples requires a complex gear meshing mechanism modelling, [22], which is not pursued in this research. However, we have shown that a Kalman filter estimation of the torque ripples, using simple harmonic oscillator model, can accurately estimate the torque ripples [19].

The output velocity and torque of the simulated system are compared to typical experimental outputs in Figure 9. For the unrestrained system, there is an almost perfect match for the velocity, and a relatively good match for torque curves, except for the torque ripples. For the restrained system, the match between velocities is less accurate compared to that for the unrestrained system, which is because of the smaller velocity signal and larger noise–to–signal ratio. However, the resulting torques are quite similar and there is no torque ripple observed for the restrained system. This accurate match was verified

for more than twenty other experiments for both harmonic drives, and similar results are obtained for both restrained and unrestrained systems. The accurate match between simulation and experiment for different operating ranges, indicates the fidelity of the model to accurately replicate the dynamic behavior of the system, and confirmed the effectiveness of modelling and parameter identification schemes to capture the dynamics of the harmonic drive systems.

To realize the significance of the nonlinear model and compare it to simpler models, a simulation study was done in which, for a set of experiments, the simulation results of the complete model is compared to that of the simplified model. In this study the importance of Coulomb, viscous, and Stribeck model for friction as well as structural damping model has been examined. It is concluded that Coulomb friction plays the most important role for both high– and low–velocity experiments, while the effect of viscous friction is more vital at high–velocity experiments, and Stribeck friction is only important at very low velocity experiments. Moreover, the structural damping model contributes significantly to estimate both velocity and torque output of the system accurately. Figure 10 illustrates a typical velocity comparison of this study, where the significance of Coulomb friction and structural damping to estimate the velocity of the system is shown separately.

5 Conclusions

Based on experimental and theoretical studies, a systematic way to capture and rationalize the dynamics of the harmonic drive systems is introduced. Simple and accurate models for compliance, hysteresis, and friction are established and model parameters are identified using least–squares approximation. A measure of variation is defined, by which the reliability of the estimated parameter for different operating condition, as well as the accuracy of the simple model is quantified. From compliance modelling results, it has been shown that identifying stiffness and structural damping together will resolve the reported difficulties in determining the compliance parameters. Moreover, it has been shown that a linear stiffness model best captures the behavior of system when combined with a good model for hysteresis. A simple static model for hysteresis is also introduced, and it is shown that this simple model can replicate the hysteresis effect in harmonic drives better than some other more complex dynamic models reported in the literature. Friction losses of the harmonic drive are modelled at both low and high velocities. From experiments on two different harmonic drives it has been observed that there is no stiction in the

transmission, but rather a rising friction acts at low velocities. Finally, the model performance is assessed by a simulation verifying the experimental results for both restrained and unrestrained systems.

References

[1] N.A. Aliev. A study of the dynamic behavior of flexible gears in harmonic drives. *Soviet Eng. Res.*, 66(6):7–11, 1986.

[2] B. Armstrong-Helouvry. Stick slip and control in low speed motion. *IEEE Trans. on Aut. Cont.*, 38(10):1483–1496, October 1993.

[3] B. Armstrong-Helouvry, P. Dupont, and C. Canudas de wit. A survey of models, analysis tools and compensation methods for control of machines with friction. *Automatica*, 30(7):1083–1138, 1994.

[4] A. Ben-Israel. *Generalized Inverses: Theory and Application.* Wiley, New York, 1974.

[5] J.H. Charlson. Harmonic drives for servomechanisms. *Machine design*, 57(1):102–106, January 1985.

[6] P.R. Dahl. Solid friction damping of mechanical vibration. *AIAA J.*, 14(12):1675–1682, December 1976.

[7] K.L. Doty, C. Melchiorri, and C. Bonivento. Theory of generalized inverses applied to robotics. *Int. J. Rob. Res.*, 12(1):1–19, Feb 1993.

[8] G.H. Golub and C. Van Loan. *Matrix computations.* The Johns Hopkins University Press, Baltimore, MD, 1983.

[9] M. Hashimoto, Y. Kiyosawa, H. Hirabayashi, and R.P. Paul. A joint torque sensing technique for robots with harmonic drives. *Int. Conf. Robotics and Automation*, pages 1034–1039, April 1991.

[10] D.P. Hess and A. Soom. Friction at a lubricated line contact operating at oscillating sliding velocities. *J. Tribology*, 112(1):147–152, January 1990.

[11] L. Hsia. The analysis and design of harmonic gear drives. *Int. Conf. Systems, Man and Cybernetics*, 1:616–619, 1988.

[12] HD Systems Inc. Harmonic drive gearing. *HD Systems Catalogue*, 1991.

[13] N. Kircanski, A. Goldenberg, and S. Jia. An experimental study of nonlinear stiffness, hysteresis, and friction effects in robot joint with harmonic drives and torque sensors. *Int. Symp. Exp. Rob.*, 1:147–154, 1993.

[14] G. legnani and R. Faglia. Harmonic drive transmission: the effect of their elasticity, clearance and irregularity on the dynamic behaviour of an actual SCARA robot. *Robotica*, 10:369–375, October 1992.

[15] J.W. Macki, P. Nistri, and P. Zecca. Mathematical models for hysteresis. *SIAM Review*, 35(1):94–123, March 1993.

[16] T. Marilier and J.A. Richard. Non-linear mechanic and electric behavior of a robot axis with a harmonic-drive gear. *Robotics and Computer-Integrated Manufacturing*, 5(2/3):129–136, 1989.

[17] W. Seyfferth, A.J. Maghzal, and J. Angeles. Nonlinear modelling and parameter identification of harmonic drive robotic transmissions. *Int. Conf. Rob. Aut.*, 3:3027–3032, 1995.

[18] H.D. Taghirad. On the modelling and identification of harmonic drive systems. *CIM Internal Report*, 1995.

[19] H.D. Taghirad, A. Helmy, and P.R. Belanger. Intelligent built-in torque sensor for harmonic drive system. *To be presented in the 1997 IEEE Instrumentation and Measurement Technology Conference*, May 1997.

[20] D.C. Threlfall. The inclusion of coulomb friction in mechanisms programs with particular reference to DRAM. *Mech. and Mach. Theory*, 13:475–483, 1978.

[21] A. Tustin. The effects of backlash and speed-dependent friction on the stability of closed-cycle control systems. *J. Inst. Elec. Eng.*, 94(2A):143–151, 1947.

[22] T.D. Tuttle. Understanding and modelling the behavior of a harmonic drive gear transmission. Technical Report 1365, MIT Artificial Intelligence Laboratory, 1992.

[23] T.D. Tuttle and W.P. Seering. A nonlinear model of a harmonic drive gear transmission. *IEEE Transaction on Robotics and Automation*, 12(3):368–374, June 1996.

[24] D.P. Volkov and Y.N. Zubkov. Vibration in a drive with harmonic gear transmission. *Russian Engineering J.*, 58(5):17–21, 1978.

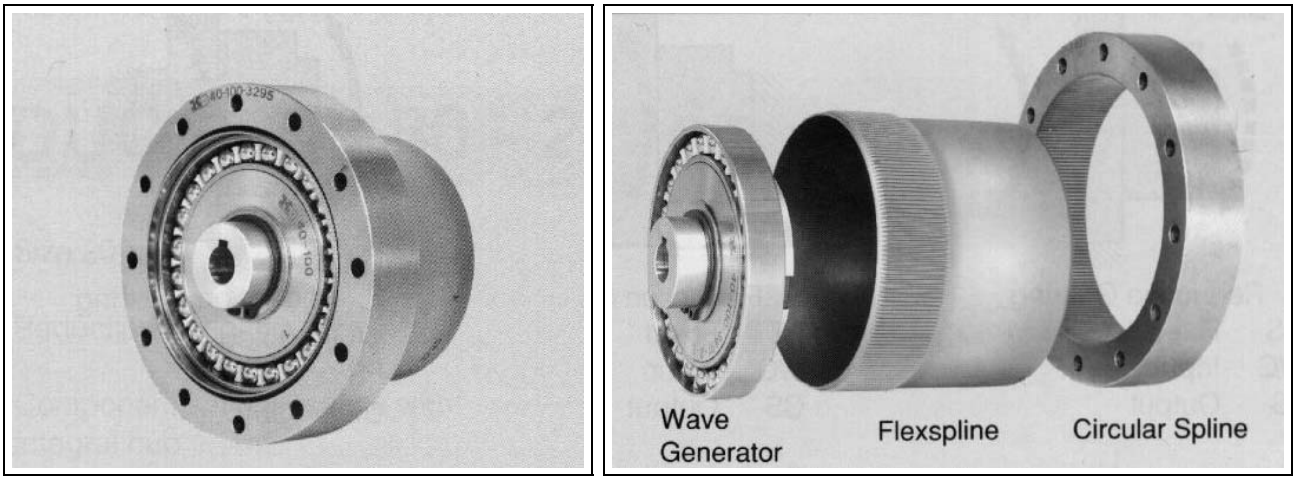

Figure 1: Harmonic drive components

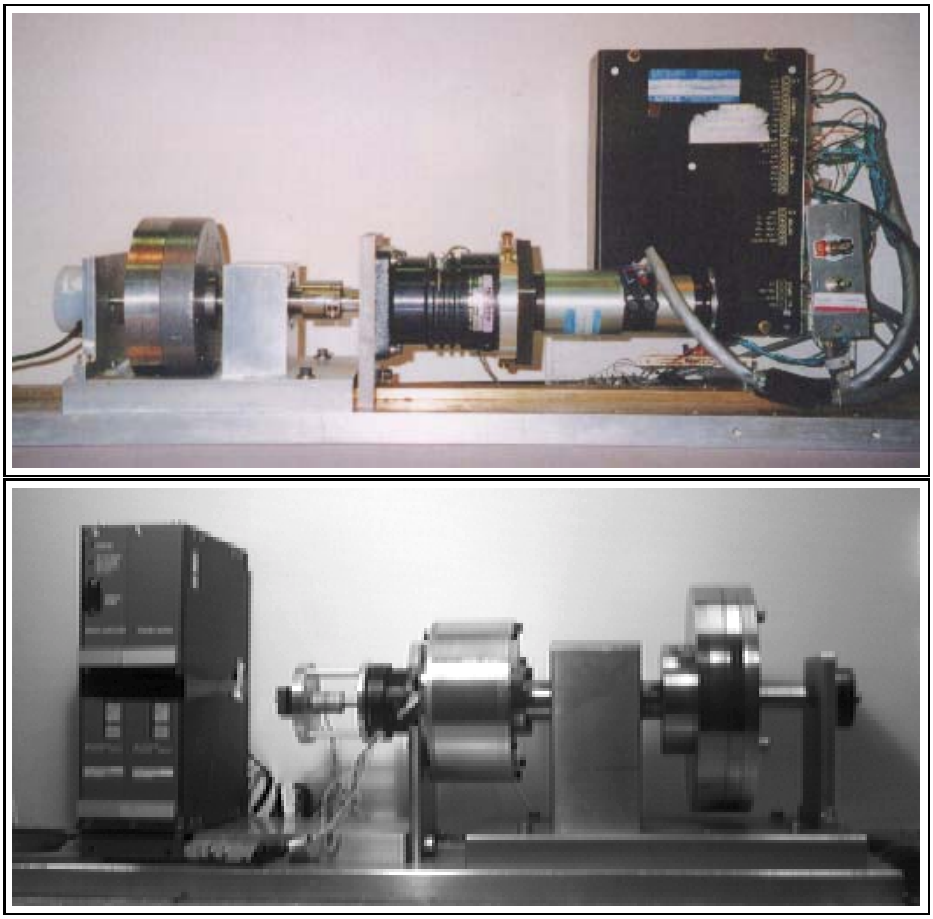

Figure 2: A picture of the experimental setups for the two harmonic drives

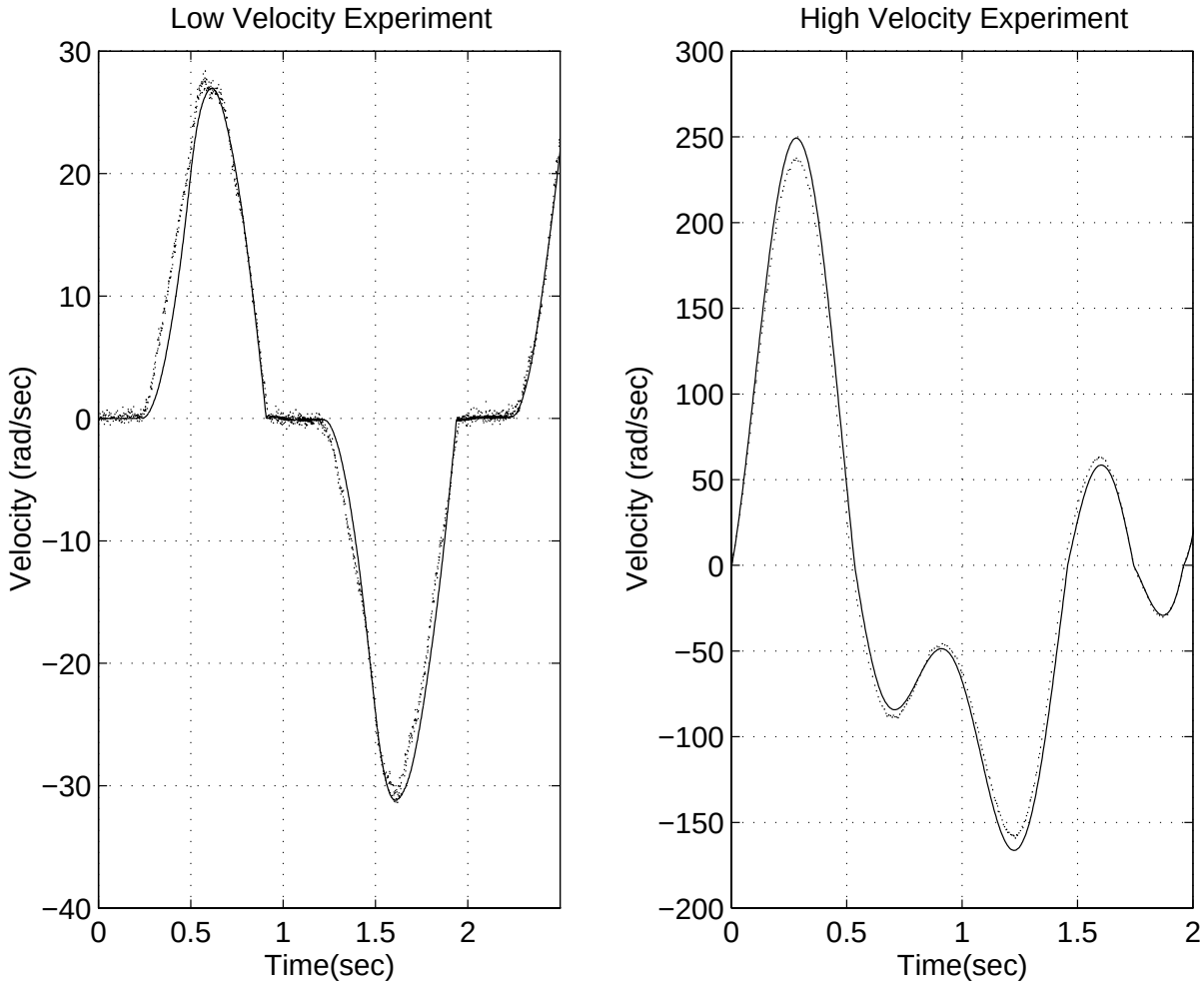

Figure 3: Velocity comparison of the model and experiment for two typical experiments; Solid: simulations, dotted: measured velocity

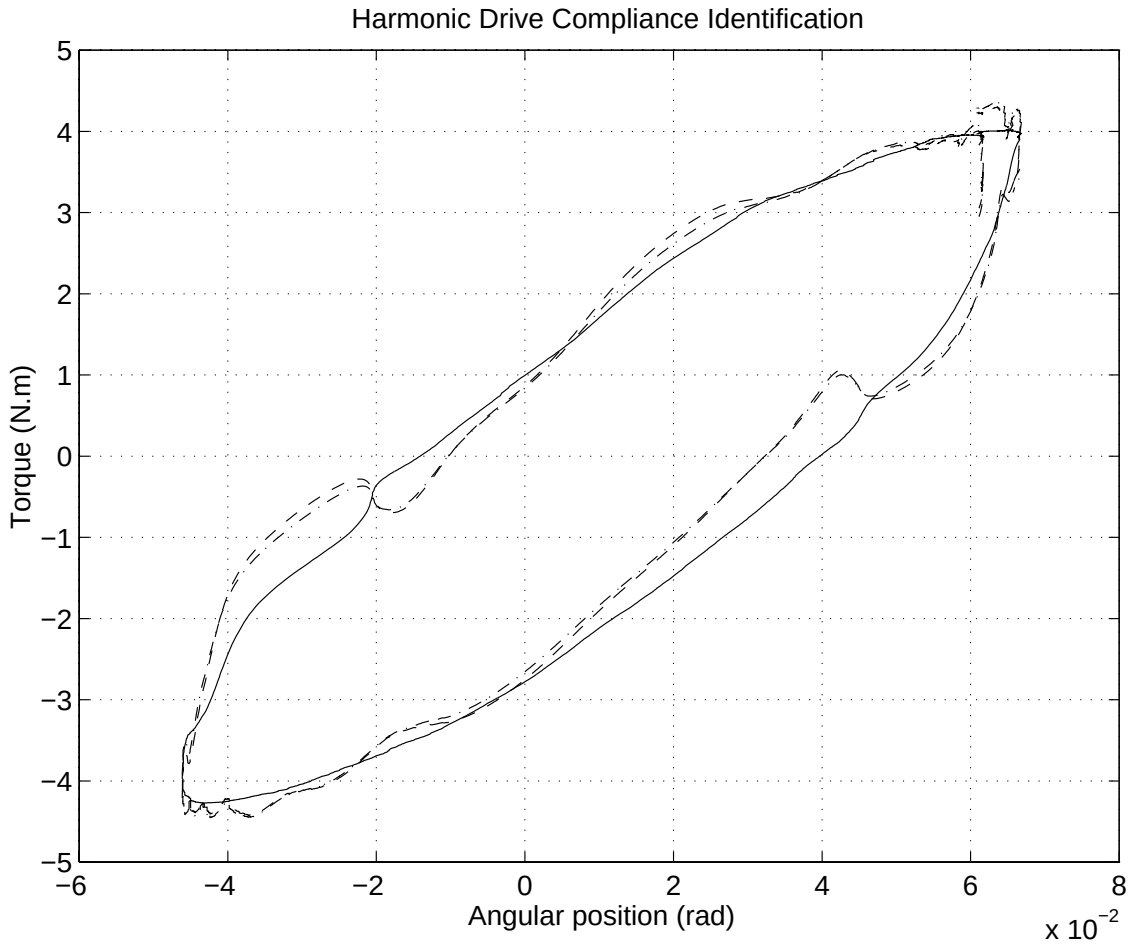

Figure 4: Typical hysteresis curve and its model for optimal α (dash-dot), and $\alpha = \frac{1}{2}$ (dashed)

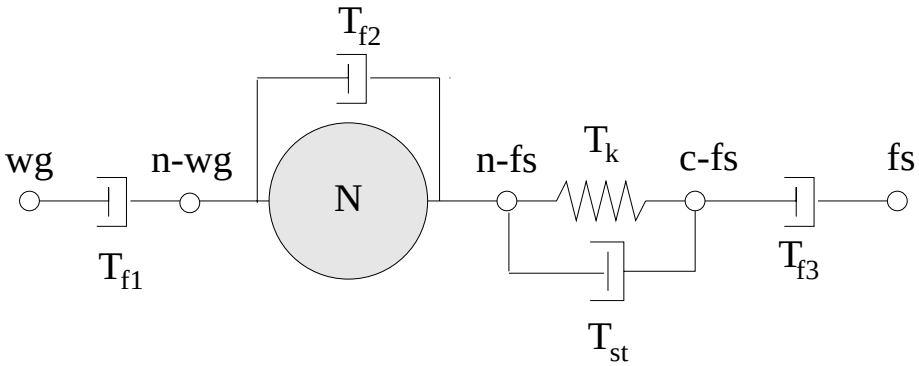

vvvv

Figure 5: *Transmission model of harmonic drive with compliance and friction*

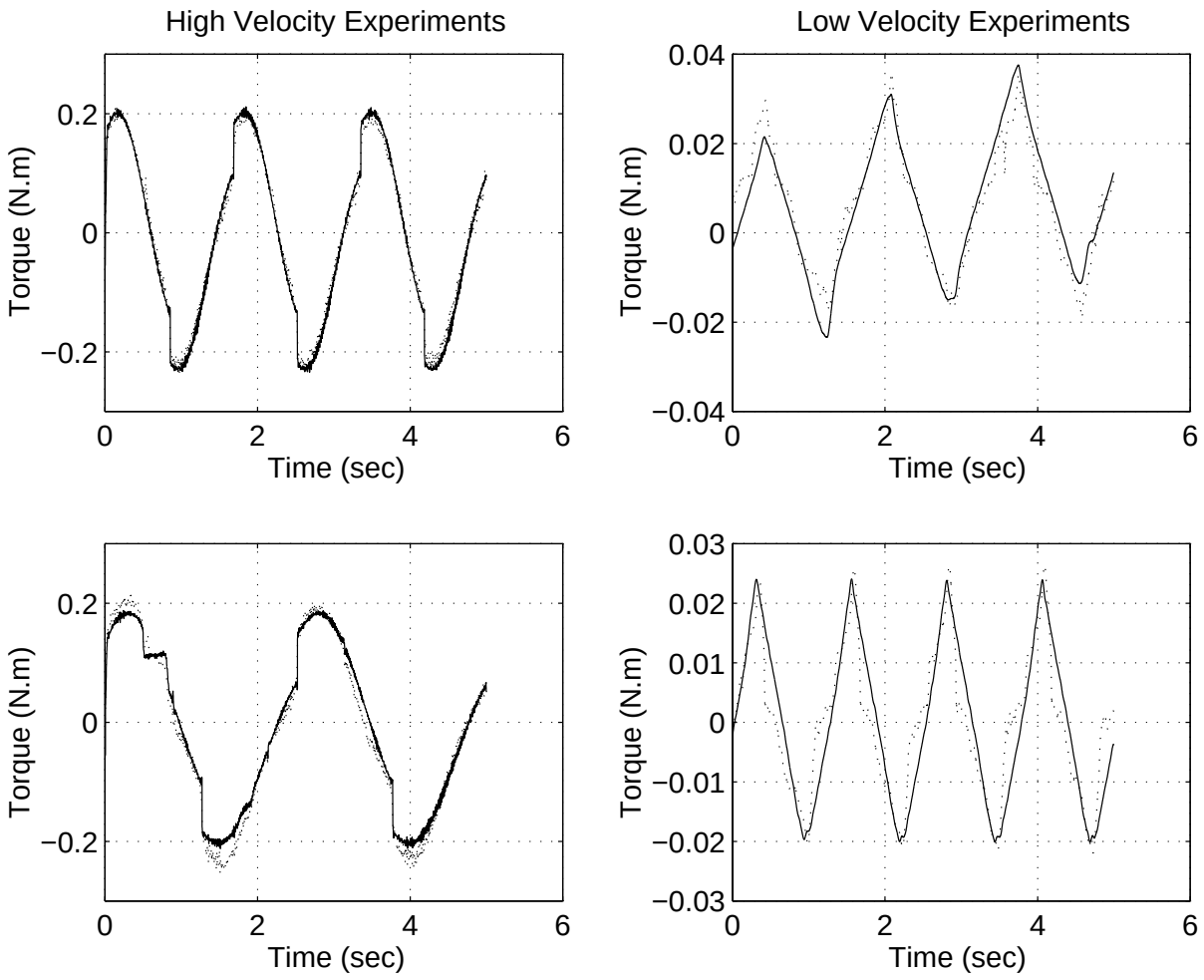

Figure 6: Comparison of output torque in simulations and experiments; dotted: experiment, solid: simulation

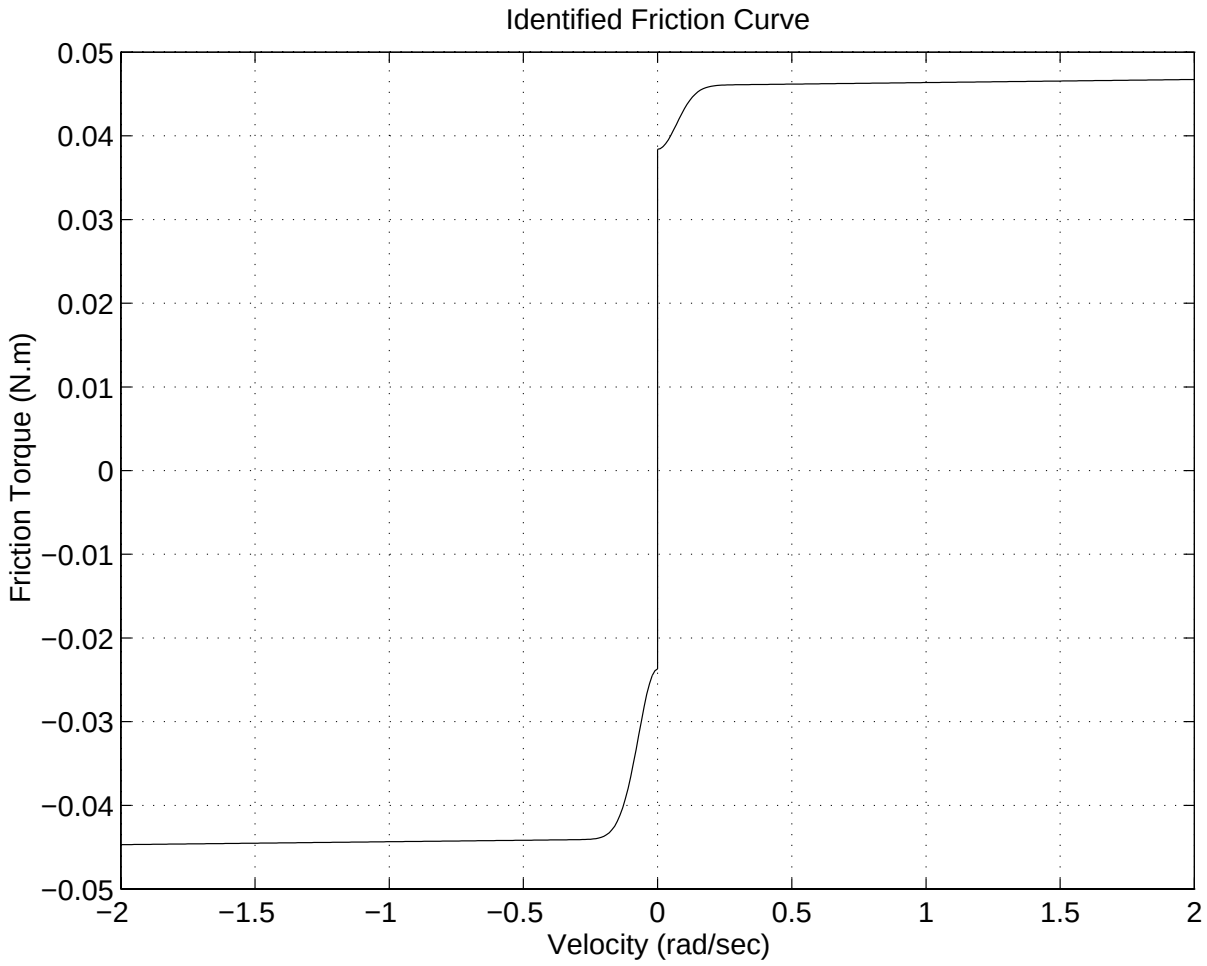

Figure 7: Identified friction curve

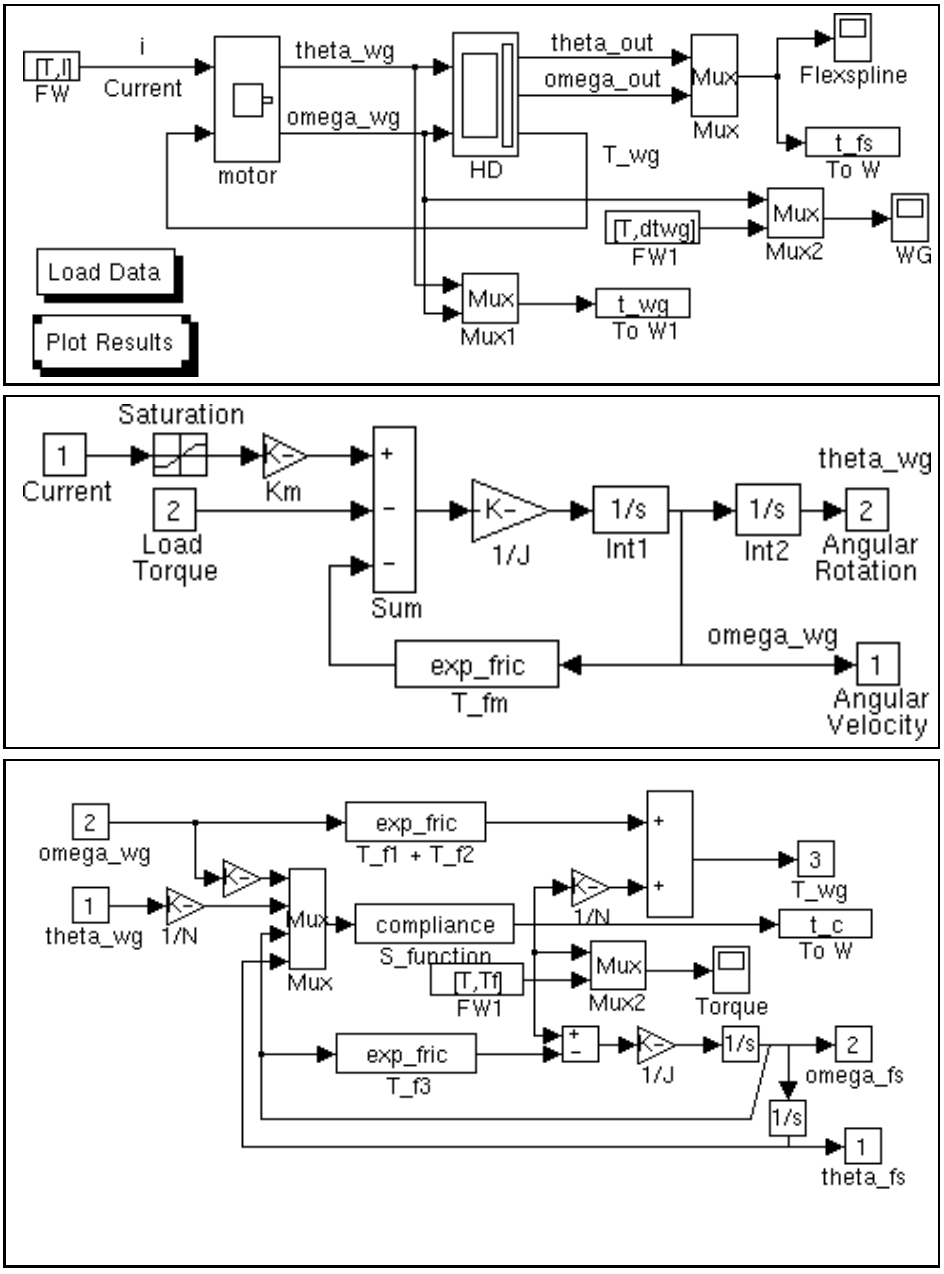

Figure 8: Unrestrained system simulated on Simulink for model verification purpose. Top: System; Mid: DC–motor; Bot: Harmonic drive

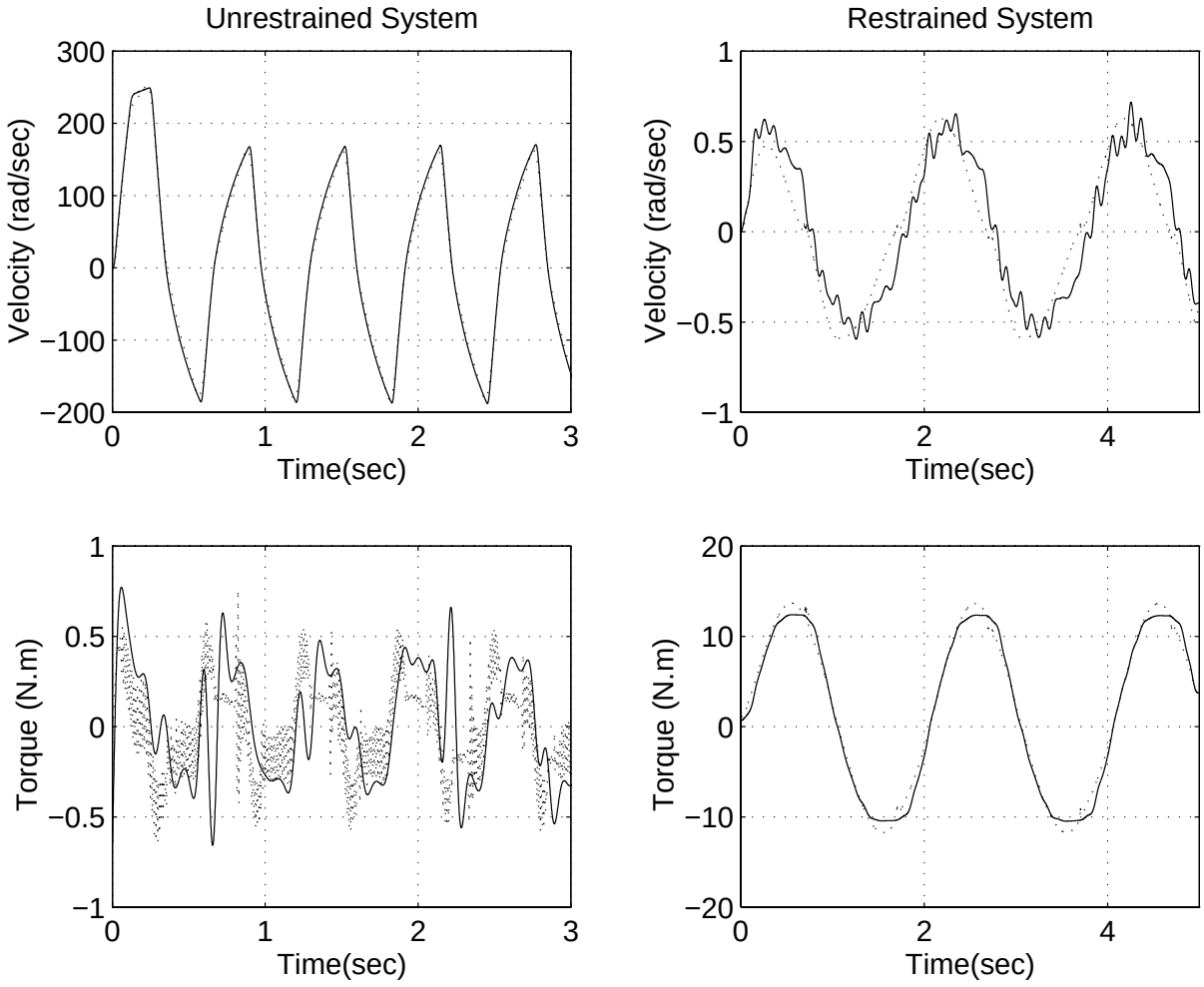

Figure 9: Simulation verification for unrestrained and restrained systems; Solid : Simulation, Dotted : Experiment

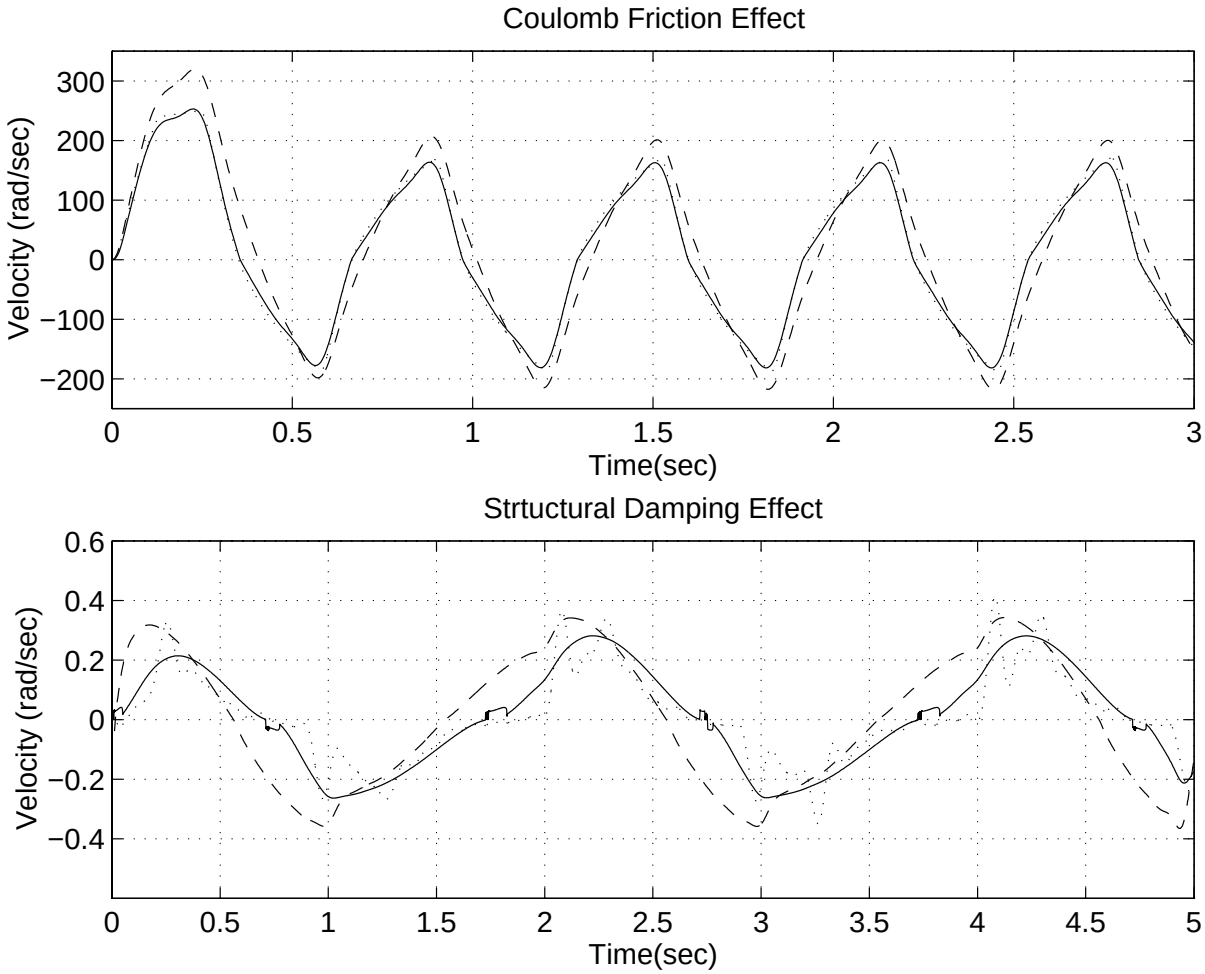

Figure 10: Velocity comparison of the experiment with the complete and simplified model, where the significance of Coulomb friction (top), and structural damping (bottom) are examined separately; Dotted : Experiment, Solid : Complete model, Dashed : Simplified model

List of Figures